ResearchGate

See discussions, stats, and author profiles for this publication at: https://www.researchgate.net/publication/231411358

Intrazeolite Metal Carbonyl Phototopotaxy: From Tungsten (VI) Oxide Quantum Dots to a Zero-Dimensional Semiconductor Quantum Supralattice

ARTICLE *in* THE JOURNAL OF PHYSICAL CHEMISTRY · SEPTEMBER 1990

Impact Factor: 2.78 · DOI: 10.1021/j100382a046

CITATIONS
32

READS
13

2 AUTHORS, INCLUDING:

Saim Özkar
Middle East Technical University
298 PUBLICATIONS **5,282** CITATIONS

SEE PROFILE

Available from: Saim Özkar
Retrieved on: 24 January 2016

Intrazeolite Metal Carbonyl Phototopotaxy: From Tungsten(VI) Oxide Quantum Dots to a Zero-Dimensional Semiconductor Quantum Supralattice

Geoffrey A. Ozin* and Saim Özkar†

Lash Miller Chemistry Laboratory, University of Toronto, Toronto, Ontario, Canada M5S 1A1
(Received: November 7, 1989; In Final Form: April 11, 1990)

Attention is focused on the use of simple binary metal carbonyls for the nucleation, growth, and stabilization of intrazeolite semiconductor quantum nanostructures. The rationale for selecting this particular group of precursor molecules relates to their volatility, molecular dimensions, ease of purification, availability, and facile and quantitative conversion to the respective metal oxide materials with minimal contamination by carbon. In this study the intrazolite photooxidation chemistry of α-cage encapsulated hexacarbonyltungsten(0) in $Na_{56}Y$ and $H_{56}Y$, $n\{W(CO)_6\}$-$Na_{56}Y(H_{56}Y)$, with O_2 provides a novel synthetic pathway to α-cage-located tungsten(VI) oxide $n(WO_3)$-$Na_{56}Y(H_{56}Y)$ intrazeolite quantum dots and a zero-dimensional semiconductor quantum supralattice (where n = 0-32), which might find applications as new solid-state materials for use in quantum electronic and nonlinear optic devices.

Introduction

One of the key issues in the microfabrication of semiconductor quantum nanostructures is the maintenance of sharp boundaries or interfaces between organized assemblies of quantum objects with precisely defined size and dimensionality (called quantum wells, wires, and dots).[1] By using a photon source to dissociate one or more of the precursors, deposition and epitactic growth of 2-D quantum confined layered superlattices can often be accomplished at *lower substrate temperatures* than by thermal epitaxy, thereby preventing atomic diffusion.[2] This brief paper describes a novel intrazeolite topotactic photooxidation reaction:

$$n\{W(CO)_6\}\text{-}ZY + {}^9/_2 nO_2 \xrightarrow{h\nu} n(WO_3)\text{-}ZY + 6nCO_2$$

(where n = 0-32; ZY = $Na_{56}Y$ or $H_{56}Y$, denoted $Na_{56}Y(H_{56}Y)$) which permits the mild, clean and controlled intrazeolite nucleation, growth, and organization of zero-dimensional $(WO_3)_{2,4}$ quantum dots into a zero-dimensional quantum supralattice[27] built of $(WO_3)_{2,4}$ quantum dots. *Thermal* synthetic pathways to intrazeolite quantum dots, wires, and supralattices have recently been reported.[3]

Recall that the various allotropic modifications of bulk tungsten(VI) oxide all contain the common structural feature of corner sharing octahedral basic building blocks.[4] The numerous stable WO_3 phases that occur between 10 and 1200 K have more or less distorted ReO_3 structures. The most well-known monoclinic (290-603 K) phase m-WO_3 is made up of corner-sharing distorted and tilted WO_3 octahedra. It is an allowed-indirect bandgap semiconductor, E_g = 2.7 eV, with fascinating solid-state ion insertion, electronic/ionic transport, electrochromic, and nonstoichiometry properties.[4] The metastable hexagonal modification h-WO_3 contains essentially undistorted corner-sharing octahedra. This structure supports large hexagonal channels running down the c axis of the crystal, formed by stacking infinite planes of WO_6 units arranged in the form of six-membered rings.[4]

Experimental Section

Materials. The high-purity, crystalline sodium zeolite Y host with the unit cell composition $Na_{56}(AlO_2)_{56}(SiO_2)_{136}\cdot xH_2O$ was obtained from Dr. Edith Flanigen at Union Carbide, Tarrytown, NY. To remove cation defect sites, thermally dehydrated/calcined $Na_{56}Y$ was slurried with 0.01 M NaCl, 0.01 M NaOH solution and washed until free of Cl^-. $(NH_4)_{56}Y$ and $H_{56}Y$ were prepared by the use of standard ion-exchange techniques and deammination procedures.[5] All zeolite samples were stored over saturated NH_4Cl solution to ensure a constant humidity until use. $W(CO)_6$ was purchased from Strem Chemicals, Inc., Newburyport, MA.

Spectroscopic Cells and Equipment. The work reported in this paper used specially designed cells for complete in situ treatments. The combined mid-IR transmission/UV-visible reflectance cell basically consists of a Pyrex tube with NaCl infrared windows at one end joined via a metal O-ring sealed flange to a dehydration quartz tube at the other end.[6] Thermal treatments in the quartz tube section of the cell can be carried out up to temperatures of about 500 °C. The zeolite wafers are supported in a stainless steel holder that can easily be moved into place between the NaCl or quartz windows to obtain a mid-IR transmission or UV-visible reflectance spectrum at any point of the experiment. Two greaseless stopcocks allow for the organometallic sample to be attached at one side of the cell and a vacuum applied at the other during organometallic vapor-phase impregnation of the zeolite wafer. Alternatively, the cell can be attached to a gas line for the introduction of reactants such as O_2 or CO.

Spectrometers. The mid-IR spectra were obtained on a Nicolet 20SXB FTIR spectrometer. All spectra presented have been obtained by subtraction of the initial spectrum of the dehydrated zeolite from the organometallic-impregnated sample, followed by baseline correction. Far-IR spectra were obtained on a Nicolet 20F FTIR spectrometer. Optical reflectance spectra were obtained on a Perkin-Elmer 330 spectrometer using a $BaSO_4$ disk as reference. Powder XRD patterns were recorded on a Phillips PW 1051 and a Scintag PADX θ-θ diffractometer using Ni filtered Cu Kα radiation (1.541 78 Å). The Scintag equipment was interfaced with a Digital Corp. Microvax II computer running

† On sabbatical leave from the Chemistry Department, Middle East Technical University, Ankara, Turkey.

(1) Herman, I. P. *Chem. Rev.* **1989**, *89*, 1323, and references therein.
(2) Almond, M. J.; Rice, D. A.; Yates, C. A. *Chem. Br.* **1988**, *24*, 1130, and references therein.
(3) Ozin, G. A.; Stein, A.; Stucky, G. D. *J. Am. Chem. Soc.* **1990**, *112*, 904. Ozin, G. A.; Kuperman, A.; Stein, A. *Adv. Mater.* **1989**, *101*, 373. Stein, A.; Ozin, G. A.; Stucky, G. D. *J. Soc. Photogr. Sci. Technol. Jpn.* **1990**, *53*, 1. Ozin, G. A.; Stein, A.; Stucky, G. D.; Godber, J. G. *J. Inclusion Phenom.*, in press. Ozin, G. A.; Stein, A.; Godber, J. G. U.S. Patent 4,942,119, July 17, 1990. Wang, Y.; Herron, N. *J. Phys. Chem.* **1987**, *91*, 257. Wang, Y.; Eddy, M. M.; Stucky, G. D.; Cox, D. E.; Moller, K.; Bein, T. *J. Am. Chem. Soc.* **1989**, *111*, 530. Moller, K.; Eddy, M. M.; Stucky, G. D.; Herron, N.; Bein, T. *J. Am. Chem. Soc.* **1989**, *111*, 2569. Wang, Y.; Herron, N. *J. Phys. Chem.* **1987**, *91*, 5005. *Ibid.* **1988**, *92*, 4988. Thomas, J. K.; Stramel, R. D.; Nakamura, T. *J. Chem. Soc., Faraday Trans. 1* **1988**, *84*, 1287. Parise, J. B.; MacDougall, J.; Herron, N.; Farlee, R.; Sleight, A. W.; Wang, Y.; Bein, T.; Moller, K.; Moroney, L. M. *Inorg. Chem.* **1988**, *27*, 221. MacDougall, J. E.; Eckert, H.; Stucky, G. D.; Herron, N.; Wang, Y.; Moller, K.; Bein, T.; Cox, D. *J. Am. Chem. Soc.* **1989**, *111*, 8006. Terasaki, O.; Yamazaki, K.; Thomas, J. M.; Ohsuna, T.; Watanabe, D.; Sanders, J. V.; Barry, J. C. *Nature* **1987**, *330*, 58. Bogomolov, V. N.; Kholodkevich, S. V.; Romanov, S. G.; Agroskin, L. S. *Solid State Commun.* **1983**, *47*, 181. Tamura, K.; Hosokawa, S.; Endo, H.; Yamasaki, S.; Oyanagi, H. *J. Phys. Soc. Jpn.* **1986**, *55*, 528. Stucky, G. D.; MacDougall, J. E. *Science* **1990**, *247*, 669.
(4) Rao, C. N. R.; Gopalakrishnan, J. *New Directions in Solid State Chemistry*; Cambridge University Press: Cambridge, 1986. Adams, D. M. *Inorganic Solids*; Wiley: London, 1979. West, A. R. *Solid State Chemistry and Its Applications*; Wiley: Chichester, 1984, and references therein.
(5) Dwyer, J.; Dyer, A. *Chem. Ind.* **1984**, *237*, and references therein.
(6) Ozin, G. A.; Godber, J. G. *J. Phys. Chem.* **1988**, *92*, 4980.

0022-3654/90/2094-7556$02.50/0 © 1990 American Chemical Society

associated software. ^{29}Si MAS NMR spectra of solid samples were recorded on a Chemagnetics CMX-300 at 59.7 MHz. Solid-state EPR data were collected on a Bruker ESP-300 spectrometer. XPS experiments were performed at the University of Western Ontario, Surface Science Laboratory Facility, using a SSX-100 system. Raman data were obtained on a Jobin Yvone Instrument SA spectrometer, using a Coherent Model Innova 90 Ar ion pump and Coherent Model CR 559 dye lasers as the excitation source.

The details of the XPS experiments require some discussion. The SSX-100 system utilizes monochromatic Al Kα X-rays capable of being focused to a spot size of 150 μm, and a pass energy of 148 eV was used. The electron takeoff angle was kept constant at 35°. Binding energies have been corrected for the shifts observed due to sample charging and spectra are referenced to the C(1s) hydrocarbon component, which was assigned the value of 284.9 eV.[7] Quantitative elemental composition measurements were made by correction of integrated peak intensities with the Scofield factors[8] modified to take account of differences in photoelectron mean free path for a given kinetic energy ($\lambda \propto E_k^{0.7}$). Peak envelopes were fitted with a least-squares routine employing an 80% Gaussian peak shape and using the Shirley baseline correction. To control the charging effect that results in binding energy shifts and broadening of all photoelectron peaks, the electron flood gun/screen technique was employed.[9] Thus by placing a conducting Ni mesh within 1 mm of the sample surface and employing an electron flood gun, line widths of 1.5 eV (fwhm) have been achieved for the C(1s) peak. The W(4f) high-resolution spectra employed a spot size of 150 μm and a pass energy of 50 eV.

Experimental Procedure. About 20 mg of size-sieved zeolite crystals are pressed into a self-supporting wafer with a diameter of 16 mm by applying a pressure of 5 tons/in^2 for 10 s. The disks are secured in the stainless steel sample holder and placed in the quartz part of the cell. The thermal dehydration of the wafer under dynamic vacuum, using an Omega Series CN-2010 programmable temperature controller, follows a preset temperature schedule: 25–100 °C over 1 h, 1 h at 100 °C, 100–450 °C over 3 h, and 1 h at 450 °C. This was followed by calcination in a static atmosphere of 300 Torr of oxygen at 450 °C for 1 h and pumping hot at this temperature. The degree of dehydration was judged by the flatness of the baseline in the IR ν(OH) stretching and δ(OH) deformation regions, 3400–3700 and 1600–1650 cm^{-1}, respectively. When a sufficiently dehydrated sample was obtained, the wafer was moved into place above the organometallic sample holder. By opening the stopcock to the sample holder, exposure to the organometallic vapor under dynamic vacuum was continued until the desired absorbance was obtained in the carbonyl mid-IR region.

For the photoreactions, the wafer was irradiated in the quartz part of the mid-IR transmission/UV–visible reflectance cell by using a 450-w high-pressure xenon arc lamp (OSRAM XBO), a 10-cm water cell IR filter, and a $\lambda < 245$ nm cutoff filter of oxygen. In the case of, for example, a zeolite wafer containing four molecules of $W(CO)_6$ per unit cell, the photooxidation reaction was completed within 1 h. A digital radiometer capable of reading as little as 1 μW cm^{-2} demonstrates transmission of photons through a homogeneously exposed wafer. The photokinetic behavior is reproducible and well behaved. It would appear that all zeolite crystals are equally exposed in our photooxidation reaction of n\{$W(CO)_6$\}–$Na_{56}Y(H_{56}Y)$ to $n(WO_3)$–$Na_{56}Y(H_{56}Y)$.

Elemental analyses for Na, Al, and W were performed by neutron activation analysis on the University of Toronto Slow Poke Reactor.

Results and Discussion

Gaseous $W(CO)_6$ absorbs into vacuum thermally dehydrated $Na_{56}Y$ and $H_{56}Y$ at room temperature to give a saturation loading of 2 $W(CO)_6/\alpha$-cage, corresponding to 16 $W(CO)_6$/unit cell (elemental analysis). Effective size exclusion of $W(CO)_6$ by 3-Å window size K_8Na_4-A confirms that $W(CO)_6$ is confined *internally* in zeolite Y.[10] The homogeneity of the distribution of $W(CO)_6$ in the zeolite Y crystals is established by the *selective and complete* hydrogen bonding (mid-IR) of $W(CO)_6$ to the α-cage protons in $H_{56}Y$ (four Brønsted protons/α-cage[11]). The observation of IR activity for *all six* ν(CO) fundamentals of $W(CO)_6$, taken together with a maximum filling of 2 $W(CO)_6/\alpha$-cage in both $Na_{56}Y$ and $H_{56}Y$ (four sodium cations and protons per α-cage[10,11]) signals a *trans*-ZONa(H)···OCW(CO)$_4$CO···(H)NaOZ anchoring site geometry with C_{2v} or lower symmetry for encapsulated $W(CO)_6$. Powder XRD patterns up to saturation filling show lines exclusively of zeolite Y, thereby demonstrating that $W(CO)_6$ is *entrapped* within an *intact* zeolite Y framework. The ^{29}Si MAS NMR spectra of these $W(CO)_6$–$Na_{56}Y(H_{56}Y)$ samples are essentially those of the virgin $Na_{56}Y(H_{56}Y)$ zeolites. The XPS spectra of the same samples (Table I) clearly depict the presence of unoxidized $W(CO)_6$–$Na_{56}Y(H_{56}Y)$ (core level ionizations W(4f) = 31.0 (32.0), W(4d) = 243.9 (244.9) eV[8a] with an observed W:Na:Al elemental ratio (corrected for photoionization cross sections and instrument sensitivity factors) usually slightly less than that obtained by bulk elemental analysis. (The latter observation clearly signals that there exists no preferential adsorption of $W(CO)_6$ on, or migration to, the external surface of the zeolite. Recall that XPS is a surface-sensitive technique capable of probing to a depth of about 50 Å.[12]) The optical reflectance spectra display the characteristic intense UV MLCT bands of $W(CO)_6$–$Na_{56}Y(H_{56}Y)$.[13] One deduces from the above information that *homogeneous* dispersions of *internally* confined, *α-cage located*, and Na^+ cation (Brønsted proton) anchored $W(CO)_6$ precursors can be quantitatively prepared in $Na_{56}Y$ (and $H_{56}Y$) zeolite hosts up to a saturation loading of 16 $W(CO)_6$/unit cell.

TABLE I: Binding Energies (eV) for Tungsten in Various Systems

sample[a]	W(4d)[b]	W(4f)[b]
m\{$W(CO)_6$\}–$Na_{56}Y$	243.9	31.0
m\{$W(CO)_6$\}–$H_{56}Y$	244.9	32.0
WO_3 (bulk)	246.8	35.9
$n(WO_3)$–$Na_{56}Y$	247.8	36.9
$n(WO_3)$–$H_{56}Y$	248.8	37.9

[a] $m \leq 16$; $n \leq 32$. [b] Binding energies have been corrected for the shifts observed due to sample charging and are referenced to the C(1s) hydrocarbon component, which was assigned the value of 284.9 eV.[7] Binding energies were reproducible to within ±0.2 eV.

Exposure of $W(CO)_6$–$Na_{56}Y(H_{56}Y)$ samples to 400 Torr of dry O_2 at room temperature (in the dark) causes no alteration of any of the aforementioned guest–host spectral properties. However, a brief exposure to $\lambda > 240$ nm causes rapid bleaching of the diagnostic IR, UV, and XPS absorptions of $W(CO)_6$–$Na_{56}Y(H_{56}Y)$ with replacement by those of intrazeolite CO_2 (mid-IR, W:CO_2 = 1:6), the appearance of a new strong UV band peaking around 285 (300) nm with an absorption threshold estimated at 3.5 (3.1) eV (see later) and new XPS core level ionizations (Table I) at W(4f) = 36.9 (37.9), W(4d) = 247.8 (248.8) eV (with no evidence of carbon incorporation into the product down to the 1000 ppm level), clearly characteristic of photooxidation of W(0) to W(VI).[14] The W:CO_2 = 1:6 ratio was determined by a combination of W elemental analysis and CO_2 mid-IR quantitative analysis. The W was obtained together with Na and Al by neutron activation analysis on the University of

(7) (a) ASTM Standard, E 105, Vol. 03.06, 1984. (b) Swift, P. *Surf. Interface. Anal.* **1982**, *4*, 47.
(8) Scofield, J. H. *J. Electron. Spectrosc.* **1976**, *8*, 129.
(9) Bryson, C. E. *Surf. Sci.* **1987**, *189/190*, 50.
(10) Ozin, G. A.; Gil, C. *Chem. Rev.* **1989**, *89*, 1749.
(11) Mortier, W. J.; Schoonheydt, R. A. *Prog. Solid State Chem.* **1985**, *16*, 1, and references therein.
(12) Pedersen, L. A.; Lunsford, J. H. *J. Catal.* **1980**, *61*, 39.
(13) Geoffroy, G. L.; Wrighton, M. S. *Organometallic Photochemistry*; Academic Press: New York, 1979. Lever, A. B. P. *Inorganic Electronic Spectroscopy*; Elsevier: Amsterdam, 1984.
(14) Wagner, C. D.; Riggs, W. M.; Davis, L. E.; Moulder, J. F.; Muilenberg, G. E. *Handbook of X-Ray Photoelectron Spectroscopy*; Perkin-Elmer: Eden Prairie, MN, 1979.

Toronto Slow Poke Reactor. Interestingly, the CO_2 was found to be entirely contained within the zeolite pores, and within the loading ranges studied its concentration was conveniently established (using the same sample as for the W determination) by quantitative mid-IR calibration procedures. The 1:6 ratio is reproducible from sample to sample. The W:O ratio for the occluded photooxidation product was found from numerous repeat elemental analyses to be exactly 1:3. (That the photooxidation product is WO_3 is not too surprising, as prolonged matrix photooxidation of $W(CO)_6/O_2$ in solid Ar at 20 K also affords WO_3 as the isolated monomer.[15]) No peaks corresponding to any subcarbonyl species nor any W(0–V) intermediate oxidation states are observed in parallel IR, XPS, and EPR experiments on these same samples. In this content it is worth mentioning that vacuum thermal decabonylation of $M(CO)_6$–$Na_{56}Y$ samples (M = Cr, Mo, W) does in fact produce mid-IR detectable $M(CO)_n$–$Na_{56}Y$ subcarbonyls which can also be *thermally* oxidized by O_2 to yield imbibed MO_x–$Na_{56}Y$ species.[16]

Powder XRD patterns of the photooxidized samples, up to and including the heaviest loadings corresponding to roughly 4 WO_3/α-cage, namely about 32 WO_3/unit cell (elemental analysis), achieved by sequential loading/photooxidation steps (*the realization of an intrazeolite living semiconductor*, see later), confirm that the integrity of the zeolite Y lattice is maintained intact and moreover show no lines signalling the presence of bulk WO_3 nor those of any other known oxide of tungsten. During this gradual filling process, the unit cell dimension of the zeolite Y host lattice shows essentially no alteration, namely 24.690 (2) to 24.694 (2) Å over the entire loading range. Also the ^{29}Si MAS NMR spectra of these same samples before and after photooxidation show very little change. In addition, the observed XPS W:Na:Al ratios for these same samples are again usually slightly less than those obtained by bulk elemental analysis. No evidence therefore exists for either lattice breakdown or migration of the tungsten(VI) oxide product to the external surface of the zeolite as a consequence of the photooxidation reaction. (Note that it is not unexpected that the W:Na:Al ratios measured by XPS for $W(CO)_6$–$Na_{56}Y(H_{56}Y)$ and WO_3–$Na_{56}Y(H_{56}Y)$ lie slightly below those anticipated from the bulk elemental analysis. Thus for α-cage encapsulation of the $W(CO)_6$ precursor, some surface depletion of tungsten is to be expected since any $W(CO)_6$ imbibed in either "part-formed or complete α-cages" located at or near the external surface of the zeolite, are likely to be removed under vacuum.) It also proved possible to collect exceptionally high quality laser Raman spectra for WO_3–$Na_{56}Y$ by using 5145-Å Ar-ion excitation over the range 50–2000 cm^{-1} (Table II). The Raman data showed the complete absence of vibrational modes attributable to either the monoclinic or hexagonal forms of bulk WO_3 (Table II).[17] *Instead one observes the growth of a what appears to be a "single" kind of intrazeolite WO_3 aggregate species over the complete volume filling range up to 32 WO_3/unit cell, displaying diagnostic terminal W=O and bridging W–O–W stretching and deformational modes (Table II).*[17]

A simple model that adequately accounts for the observed (Figure 1) linear dependence of the decay of hexacarbonyltungsten(0) log $([W(CO)_6]/[W(CO)_6]_0)$ and growth of carbon dioxide log $(1 - [CO_2]/[CO_2]_\infty)$ with photolysis time (*in excess O_2, with no detectable reaction intermediates*) considers that the $W(CO)_6$ photooxidation rate depends on the rate of photon absorption as described by the Beer–Lambert law (at low initial $W(CO)_6$ absorbance) and the quantum yield for the conversion to CO_2.[18] Note that although reaction intermediates are never observed in our $W(CO)_6$–$Na_{56}Y$ "prolonged" photooxidation experiments, it is worth mentioning that 20 K matrix photooxidation reactions of $M(CO)_6/O_2/Ar$ show that oxometal carbonyls $O_2M(CO)_4$ and $O_2M(CO)_2$ are "short" photolysis time reactive intermediates on the pathway to the respective binary metal oxide "prolonged" photolysis products.[15] Details of and alternatives to this proposed model are being explored by selective isotope labeling experiments in conjunction with various forms of spectroscopy.

Below loading values of 1 $W(CO)_6/\alpha$-cage the diagnostic UV-LMCT absorption spectrum of the photooxidation product in $Na_{56}Y$ and $H_{56}Y$ depicts a monotonically increasing population of monodispersed WO_3 clusters, that is, intensity proportional to $W(CO)_6$ filling without shifting of the threshold energy (Figure 2). (Incidently the literature contains numerous reports that monomeric and oligomeric oxotungsten(VI) species all display intense LMCT excitations in the 200–330-nm UV region[19].) It is found that the best fit for the absorption edge is obtained by using the analytical expression for the optical absorption coefficient α^{da} of a direct-allowed bandgap excitation, namely $\alpha^{da} = K(E_g$

TABLE II: Raman Spectral Data for Intrazeolite $n(WO_3)$–$Na_{56}Y$ and Bulk Monoclinic m-WO_3 and Hexagonal h-WO_3 (cm^{-1})

m-WO_3[a] (this study)	h-WO_3[b] (ref 17)	$n(WO_3)$-$Na_{56}Y$[c,d,e] (this study)	mode assgnt[f]
		897 w	ν_a(W=O)
		852 m br sh	ν_s(W=O)
	817		
803 s			
		790 s	
		727 w sh	
711 m			
		703 w	ν(O–W–O)
	690		
	645		
		605 m	
		490 s	
		468 m sh	
		443 s	
439 vvw			
		387 m br sh	δ(O–W–O)
327 w			
	320		
		284 m br sh	
268 s			
	253		
219 vvw			
184 vw			
	162		
129 s			
	108		
84 ssh	80		rot and transl phonon modes
67 vs			
		61 s br	
55 wsh			
39 msh			

[a] Distorted ReO_3 structure, containing corner-sharing distorted and tilted WO_6 octahedra.[4,17] [b] Hexagonal tunnel structure, formed from stacked infinite layers of undistorted WO_6 octahedral units arranged in the shape of six-membered rings.[4,17] [c] The structure of matrix-isolated monomeric WO_3 is triangular planar. It shows a single IR active e'ν(W=O) stretching mode at 915 cm^{-1}.[15] [d] All Raman bands of intrazeolite WO_3 grow in with essentially the same frequencies and relative intensities over the entire volume filling range $0 < n \leq 32$. [e] IR spectra of these samples show ν(W=O) stretching modes around 828 and 900 cm^{-1}. However, lower frequency IR active modes of the WO_3 cluster guest appear to be of low intensity and overlap badly with those of the zeolite host, thereby making it difficult to precisely pinpoint their location. By contrast, the Raman modes of the WO_3 cluster guest actually dominate those of the zeolite host, the latter being a very weak Raman scatterer. Interestingly, bulk m-WO_3 is an extremely strong Raman scatterer.

(15) Almond, M. J.; Downs, A. J.; Perutz, R. N. *Inorg. Chem.* **1985**, *24*, 275. Crayston, J. A.; Almond, M. J.; Downs, A. J.; Poliakoff, M.; Turner, J. J. *Inorg. Chem.* **1984**, *23*, 3051. Poliakoff, M.; Smith, K. P.; Turner, J. J.; Wilkinson, A. J. *J. Chem. Soc., Dalton Trans.* **1982**, 651.

(16) Anderson, S. L. T.; Howe, R. F. *J. Phys. Chem.* **1989**, *93*, 4913, and references therein.

(17) Daniel, M. F.; Desbat, B.; Lassegues, J. C.; Gerand, B.; Figlarz, M. *J. Solid State Chem.* **1987**, *67*, 235, and references therein.

(18) Ozin, G. A.; Parnis, J. M. *J. Am. Chem. Soc.* **1985**, *107*, 8169; *J. Phys. Chem.* **1988**, *92*, 3959.

(19) Varga, G. M.; Papaconstantinou, E.; Pope, M. T. *Inorg. Chem.* **1970**, *9*, 662. Papaconstantinou, E.; Pope, M. T. *Inorg. Chem.* **1970**, *9*, 667, and references therein.

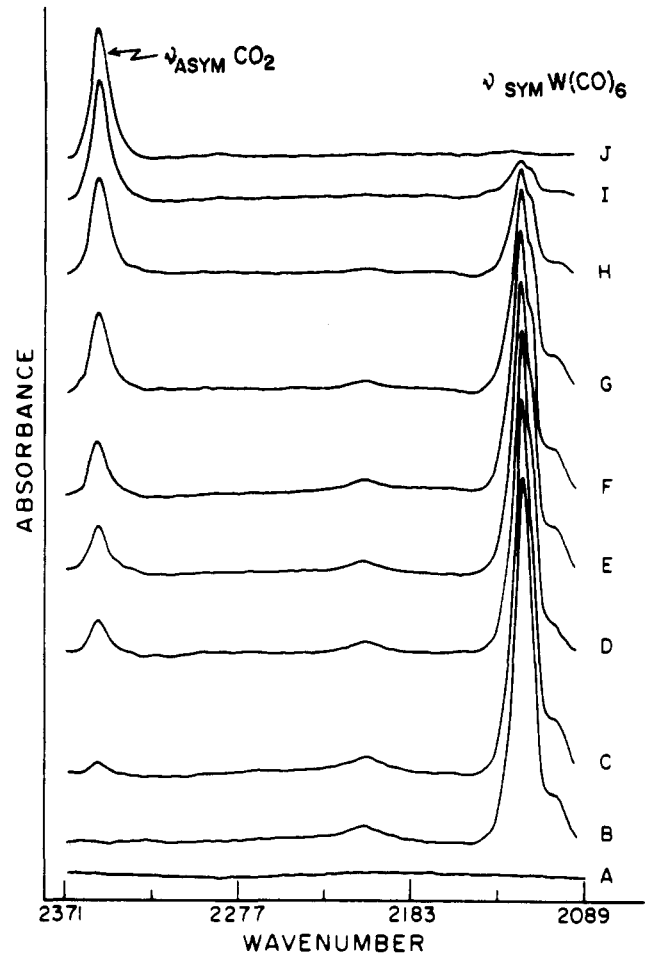

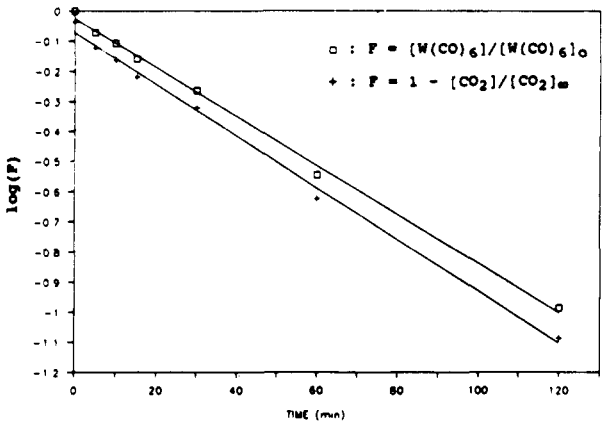

Figure 1. Time dependence of the photooxidation behaviour (mid-IR) of precursor $W(CO)_6$ and product CO_2 in the reaction $n\{W(CO)_6\}$-$Na_{56}Y + {}^9/_2 nO_2 \xrightarrow{h\nu} n(WO_3)$-$Na_{56}Y + nCO_2$.

$- E)^{1/2}$, and yields $E_g = 3.5$ (3.1) eV.[20] At and above loading values of 1 $W(CO)_6/\alpha$-cage, the aforementioned behavior begins to transform to a type in which the optical absorption intensity no longer increases significantly with filling. Furthermore the threshold energy (best fit again utilizes the expression for α^{da}) begins to red shift toward that of bulk m-WO_3 (indirect allowed bandgap, $E_g = 2.7$ eV[21]) but attaining a limiting value of E_g = 3.3 (2.9) eV for about 4 WO_3/α-cage, namely the condition for *complete volume filling* of the α-cages of zeolite Y, that is, 32

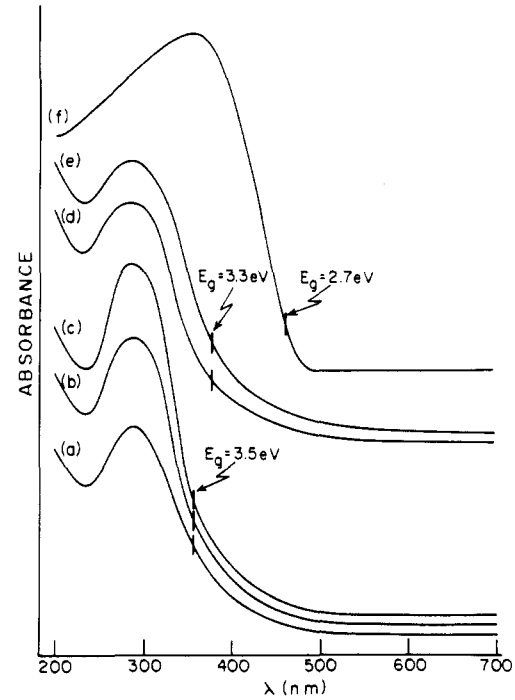

Figure 2. UV-visible absorption spectra of $n(WO_3)$-$Na_{56}Y$: (a) $n = 0.8$, (b) $n = 1.6$, (c) $n = 3.2$, (d) $n = 8.0$, (e) $n \simeq 32.0$, compared to that of (f) bulk WO_3.

(WO_3)-$Na_{56}Y(H_{56}Y)$ (Figure 2). In this context it is also noteworthy that the XPS W(4f) and W(4d) core-level ionizations are blue-shifted for both $n(WO_3)$-$Na_{56}Y(H_{56}Y)$ by 1.0 (2.0) eV, respectively, relative to those of bulk WO_3 (Table II; see later). Note that in the regime of strong quantum confinement, where the dimension of the quantum dot is smaller than that of the electron or hole lengths, one can really only make use of the effective mass approximation if one has particles that are large enough to show some measure of lattice periodicity and the beginnings of a band picture.[22] Then one can consider making use of standard expressions for direct and indirect, allowed and forbidden bandgap transitions, in order to fit the absorption edge and thereby extract a meaningful threshold energy E_g. This is the cutting edge of the field, and the physics of quantum confined particles much smaller than electron and hole lengths has not kept up with the experiments. Thus until a rigorous treatment of individual cluster systems has been resolved, the best one can do to assess variations in E_g from sample to sample is to look for a consistent and best fit to one of the standard expressions for E_g, which usually work satisfactorily for medium and weakly quantum confined semiconductor quantum nanostructures. Our reported results for E_g of $n(WO_3)$-$Na_{56}Y(H_{56}Y)$ are all obtained from computer fitting the experimental data to an $\alpha^{da} = K(E_g - E)^{1/2}$ function. The fit is remarkably good for α^{da} and superior to the others tried, namely, α^{df}, α^{ia}, and α^{if}.[20]

A scheme that explains the aforementioned sequential saturation loading/photooxidation processes observed for $n\{W(CO)_6\}$-$Na_{56}Y(H_{56}Y)$ is laid out below:

$$16W(CO)_6\text{-}Na_{56}Y(H_{56}Y) \rightarrow 16(WO_3)\text{-}Na_{56}Y(H_{56}Y) \rightarrow$$
$$8W(CO)_6,\ 16(WO_3)\text{-}Na_{56}Y(H_{56}Y) \rightarrow 24(WO_3)\text{-}Na_{56}Y(H_{56}Y) \rightarrow$$
$$4W(CO)_6,\ 24(WO_3)\text{-}Na_{56}Y(H_{56}Y) \rightarrow 28(WO_3)\text{-}Na_{56}Y(H_{56}Y) \rightarrow$$
$$\vdots \qquad\qquad \vdots$$
$$0.1W(CO)_6,\ 31.9(WO_3)\text{-}Na_{56}Y(H_{56}Y) \rightarrow 32(WO_3)\text{-}Na_{56}Y(H_{56}Y)$$

The observation of essentially complete consumption of α-cage Brønsted acid sites in a sample that analyzes closely for 32-(WO_3)-$H_{56}Y$ at full volume filling (Figure 3) nicely demonstrates that the original α-cage anchored, homogeneously distributed $W(CO)_6$ precursor yields an α-cage encapsulated WO_3 product,

(20) Burns, G. *Solid State Physics*; Academic Press: New York, 1985. Blakemore, J. S.; *Solid State Physics*, 2nd ed.; Cambridge University Press: New York, 1985.

(21) Nanthakumar, A.; Armstrong, N. R. In *Semiconductor Electrodes*; Finkleo, H. O., Ed.; Elsevier: Amsterdam, 1988, and references therein.

(22) Steigerwald, M. L.; Brus, L. E. *Annu. Rev. Mater. Sci.* **1989**, *19*, 471. Efros, A. L.; Onushenko, A. A. *Sov. Phys. Semiconduct.* **1982**, *16*, 772, and references therein.

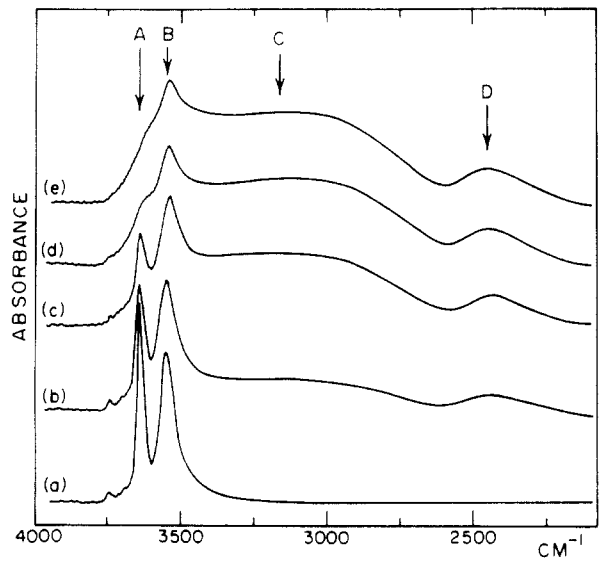

Figure 3. Series of mid-IR spectra illustrating sequential saturation loading/photooxidation events of $n\{W(CO)_6\}$-$H_{56}Y/O_2$ to yield n-(WO_3)-$H_{56}Y$ (a) $n = 0$, (b) $n = 16$, (c) $n = 24$, (d) $n = 28$, and (e) $n = 30$.

equivalently dispersed throughout the zeolite Y crystals. As described earlier, the intrazeolite aggregation process that leads to the imbibed WO_3 species yields what appears to be a *single kind* of WO_3 cluster product over the complete loading range, which in view of the analytical figures presented above of $32WO_3$/unit cell for full volume filling must be formulated as $n(WO_3)$-$Na_{56}Y(H_{56}Y)$. Here the Raman data (50–1000 cm^{-1}) for the product over the full loading range $0 < n \leq 32$ depict *only* the monotonic growth of the *same set* of diagnostic terminal W=O and bridging W–O–W stretching and deformational vibrational modes (Table II) characteristic of the creation of a *single* type of intrazeolite cluster species.[17] By inspection of Table II one can discern that this cluster species is quite distinct to that of bulk WO_3. In $H_{56}Y$ the IR spectra of the above sequence of saturation impregnation/photooxidation events (Figure 3) show a roughly stepwise halving of the absorption uptake of $W(CO)_6$ vapor together with concomitant halving of the α- and β-cage Brønsted acid site populations (labeled A and B in Figure 3). At the same time one observes parallel growth without noticeable shifting of an α-cage (strong acid) hydrogen-bonded WO_3 cluster (dioxo interaction, weak base, labeled C in Figure 3) having the bridging oxo atoms (strong base) protonated roughly in unison by the β-cage (weak acid, labeled D in Figure 3) Brønsted sites. These IR results also provide evidence for the production of what appears to be a *single kind* of intrazeolite WO_3 cluster over the full loading range.

Note that we expect bathochromic shifts on the ν(ZOH) stretching modes of the α-cage protons if they interact with the proposed WO_3 cluster. The C-band $\Delta\nu_{OH}{}^{\alpha}$ frequency shifts, breadth, and intensity are quite in line with literature results on base-induced bathochromic hydrogen-bonding shifts for α-cage Brønsted protons.[11] Also the D-band assignment to β-cage protonation of the bridging "most basic oxygen" of the proposed WO_3 cluster is quite reasonable. What is more important, is the observation that the C and D bands associated with α- and β-proton interactions with the WO_3 cluster grow in together and without noticeable frequency shifting. Simultaneously, α and β protons are consumed. Clearly we are dealing with what appears to be a *single* tungsten(VI) oxide product, namely $n(WO_3)$-$H_{56}Y$ homogeneously dispersed throughout the α-cages of the zeolite Y crystals, as seen by its interaction with *all* α- and β-cage protons at full loading, $n = 32$.

More intimate details of the aggregation picture for the conversion of $n\{W(CO)_6\}$-$Na_{56}Y(H_{56}Y)$ to $n(WO_3)$-$Na_{56}Y(H_{56}Y)$ can be obtained by performing the aforementioned sequential saturation impregnation/photooxidation experiments in $H_8Na_{48}Y$

SCHEME I: Proposed Mechanism for the Formation, Nucleation, and Growth of $n(WO_3)$-$Na_{56}Y$ ($H_{56}Y$)

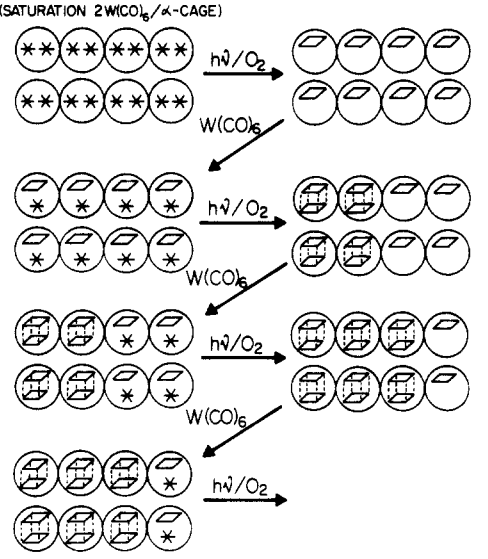

and $H_{16}Na_{40}Y$ containing one and two α-cage protons, respectively.

It is interesting to note that in these $H_8Na_{48}Y$ and $H_{16}Na_{40}Y$ experiments, one finds that both the $W(CO)_6$ precursor and WO_3 product exhibit preferential binding to two of the α-cage site II Na^+ cations, rather than to the α-cage Brønsted acid site(s). Only when one begins to exceed half-loading by precursor or product does one begin to observe hydrogen bonding to the protons in these acid zeolites. Thus the protons act as in situ hydrogen-bonding probes capable of counting the number of $W(CO)_6$ and WO_3 units contained in each α-cage. In $16\{W(CO)_6\}$-$H_8Na_{48}Y$ containing $2W(CO)_6/\alpha$-cage, hydrogen bonding of the type $ZOH_\alpha\cdots OCW(CO)_4CO\cdots NaOZ$ reduces the $\nu(OH)_\alpha$ IR band intensity to exactly *zero*. Subsequent photooxidation to $16(WO_3)$-$H_8Na_{48}Y$ *completely* restores the $\nu(OH)_\alpha$ intensity. At the $24(WO_3)$-$H_8Na_{48}Y$ stage only one-half of the $\nu(OH)_\alpha$ intensity is reinstated, at the $28(WO_3)$-$H_8Na_{48}Y$ stage one-quarter, and so on (see above). On repetition of this series of experiments with $16\{W(CO)_6\}$-$H_{16}Na_{40}Y$, hydrogen bonding of the type $ZOH_\alpha\cdots OCW(CO)_4CO\cdots H_\alpha OZ$ again reduces the $\nu(OH)_\alpha$ IR band intensity to exactly *zero*, which is subsequently restored completely in $16(WO_3)$-$H_{16}Na_{40}Y$. The process is again repeated for $n = 24$, 28, 30, where one finds that the $\nu(OH)_\alpha$ band intensity is restored to the level of one-half, one-quarter, one-eighth, and so on.

A preliminary aggregation picture for the conversion of $n\{W(CO)_6\}$-$Na_{56}Y(H_{56}Y)$ to $n(WO_3)$-$Na_{56}Y(H_{56}Y)$ that is consistent with all of our experimental observations so far is illustrated in Scheme I. Here one notes that the intrazeolite WO_3 aggregate that forms in the range up to half-loading is best formulated as the dimer $n/2(WO_3)_2$-$Na_{56}Y(H_{56}Y)$, which at $n = 16$ can be considered to exist as a quantum supralattice of dimers, namely $8(WO_3)_2$-$Na_{56}Y(H_{56}Y)$. At $n > 16$ it appears that the WO_3 dimers are gradually converted to WO_3 tetramers, which at $n = 32$ can be considered to exist as a quantum supralattice of tetramers, namely $8(WO_3)_4$-$Na_{56}Y(H_{56}Y)$. With the available data it is not possible to distinguish whether the WO_3 tetramer is actually best formulated as either a dimer of dimers or an authentic tetramer of the type illustrated in Scheme II.

The mutual spatial requirements (evaluated by CHEM-X space-filling models) and spectroscopic properties of the proposed $(WO_3)_2$ and $(WO_3)_4$ cluster guests and the α-cage of the host, with its four tetrahedrally disposed α-cage extraframework sodium cations for $Na_{56}Y$ or Brønsted protons for $H_{56}Y$,[11] are consistent with the proposed dimer–tetramer cluster inclusion models illustrated in Scheme II.[23] In this context it is worth noting the

(23) The credibility of this idea has been evaluated by EXAFS spectroscopy and Rietveld XRD powder profile analysis: Ozin, G. A.; Özkar, S.; Bein, T.; Moller, K.; Stucky, G. D. *J. Am. Chem. Soc.*, in press; work in progress.

SCHEME II

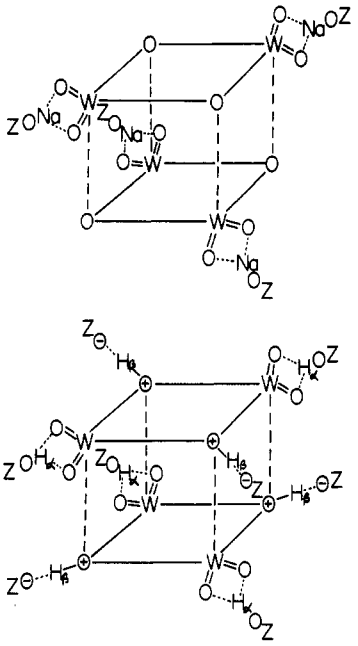

approximately 0.4-eV *red* shift observed on the optical threshold energy, together with the roughly 1.0-eV *blue* shift observed on the W(4f) and W(4d) XPS core level ionization potentials on passing from $(WO_3)_{2,4}$–$Na_{56}Y$ to $(WO_3)_{2,4}$–$H_{56}Y$. These "zeolite-induced matrix shifts" are consistent with a scheme in which the α-cage local environment of the $(WO_3)_{2,4}$ cluster is changed from that of sodium cations in $Na_{56}Y$ to that of Brønsted protons in $H_{56}Y$, as depicted in Scheme II. In $H_{56}Y$ one envisages that the combined effect of hydrogen bonding and protonation of the α-cage-encapsulated $(WO_3)_{2,4}$ cluster by α- and β-cage Brønsted acid sites, respectively, will serve to deplete the $(WO_3)_{2,4}$ cluster of electron density relative to its counterpart in $Na_{56}Y$. This will result in an overall weakening of skeletal tungsten–oxygen bonds, causing a red shift in those cluster electronic excitations of the LMCT type, as observed in the optical spectra on passing from $(WO_3)_{2,4}$–$Na_{56}Y$ to $(WO_3)_{2,4}$–$H_{56}Y$. In addition, the electronic manifold of the entire cluster will stabilize, inducing a blue shift in the W core-level ionization potentials, as observed in the XPS on passing from $(WO_3)_{2,4}$–$Na_{56}Y$ to $(WO_3)_{2,4}$–$H_{56}Y$, (Table I).[24]

A final point of considerable interest focuses attention on the 1.0 (2.0) eV blue shift in the W(4d) and W(4f) core-level ionization potentials observed on passing from $(WO_3)_{2,4}$–$Na_{56}Y(H_{56}Y)$ to that of bulk m-WO_3 respectively (Table I). This effect almost certainly can be traced to the extremely small size of the intrazeolite $(WO_3)_{2,4}$ clusters. It relates to the expected size dependence of initial (Koopman) and final (relaxation) state effects on the core-level binding energies of small clusters when in the quantum size regime.[25] Thus on passing from bulk m-WO_3 to either a $(WO_3)_{2,4}$ quantum dot or a quantum supralattice composed of $(WO_3)_{2,4}$ quantum dots, one anticipates higher ionization potentials as a consequence of (a) lower valence electron charge and lower coordination number (initial-state effect) and (b) lower valence electron screening (final-state effect).

The above data favor a nucleation and growth model for the intrazeolite phototopotactic oxidation of n[$W(CO)_6$]–$Na_{56}Y(H_{56}Y)$ by O_2 which involves the initial creation of zeolite-encapsulated and isolated $(WO_3)_2$ quantum dots, namely $n/2(WO_3)_2$–$Na_{56}Y$-$(H_{56}Y)$ ($n < 8$). As the size of the proposed $(WO_3)_2$ quantum dot is expected to be smaller than that of the bulk m-WO_3 exciton length as well as the electron and hole lengths, this loading regime is best described as having produced strongly quantum confined tungsten(VI) oxide having E_g = 3.5 (3.1) eV.[26] At $n \geq 8$ where one begins to observe red-shifting of the absorption edge to E_g = 3.3 (2.9) eV with minimal alteration of the intensity of the bandgap absorption, it appears that some kind of coupling between $(WO_3)_2$ quantum dots has ensued. In the range $8 \leq n < 32$, connectivity between $(WO_3)_{2,4}$ quantum dots evolves through the embryonic growth stages toward the genesis of an expanded tungsten(VI) oxide quantum supralattice. For *full* volume filling at n = 32, one has effectively created perfectly organized assemblies of α-cage-encapsulated $(WO_3)_4$ quantum dots running throughout the entire supercage void volume of the zeolite Y host lattice, that is, $8(WO_3)_4$–$Na_{56}Y(H_{56}Y)$, which can be considered to be either an *expanded semiconductor quantum supralattice or a zero-dimensional quantum supralattice composed of zero-dimension quantum dots.*

Preliminary high-resolution electron microscopy results (Hitachi H-600, 100 keV) provide compelling support for the above proposals.

Acknowledgment. We acknowledge the Natural Sciences and Engineering Research Council of Canada's Operating and Strategic Grants Programmes for generous financial support of this work. (S.Ö.) expresses his gratitude to the Middle East Technical University for granting him an extended leave of absence to conduct his research at the University of Toronto. Supplies of high quality Y zeolites from Dr. Edith Flanigen of U.O.P. Union Carbide, Tarrytown, NY, are gratefully appreciated. We also express our gratitude to Dr. Andrew Holmes, Dr. Neil Coombs, and Dr. Richard Prokopowicz, who assisted with the collection of the laser Raman spectra and high-resolution transmission electron microscoy data referred to in this preliminary report. We also thank all of our co-workers at Toronto for many stimulating and enlightening discussions during the course of this work.

(24) We eliminate the formation of polytungstic acids in the $H_{56}Y$ host to explain our results for several reasons. First, one requires both protons and hydroxyls to take WO_3 to H_2WO_4. One has only protons in $H_{56}Y$. Second, any formation of a strong acid like H_2WO_4 is expected to cause zeolite lattice breakdown at the high loading levels of our experiments. The powder XRD and ^{29}Si MAS NMR results definitely do not support this view. Also we know that this is not the case because control experiments that involve adding known amounts of H_2O to $(WO_3)_{2,4}$–$Na_{56}Y(H_{56}Y)$ cause the expected destruction of the integrity of the zeolite lattice with severe loss of crystallinity. For these samples XPS shows that the originally internally confined WO_3 has migrated to the external surface of the zeolite crystals. This is not the case for $(WO_3)_{2,4}$–$Na_{56}Y(H_{56}Y)$, and so polytungstic acid formation is not a likely possibility nor a viable alternative for our explanation of the shifts in the optical and XPS spectra on passing from $Na_{56}Y$ to $H_{56}Y$.

(25) Bagus, P. *J. Electron. Spectrosc.* **1985**, *36*, 257, and references therein.

(26) Brus, L. E. *J. Mater. Res.* **1989**, *4*, 704. Schmitt-Rink; Miller, D. A. B.; Chemla, D. S. *Phys. Rev. B* **1987**, *35*, 8113. Kayanuma, Y. *Phys. Rev. B* **1988**, *38*, 9797, and references therein.

(27) The term *semiconductor quantum "supralattice"* is intended to describe host–guest composite materials in which one can structurally identify *single size and shape* quantized guests, built of the atomic components of bulk semiconductors, organized in periodic arrays within the cavity and/or channel spaces of a perfectly crystalline host lattice, such as a zeolite. The unit cell dimension of the *supralattice* matches that of the host, rather than being some integral multiple of it, as is the case for a crystallographic *"superlattice"*.